Molecular Therapy
Methods & Clinical Development
Original Article

Monitoring CAR T cell generation with a CD8-targeted lentiviral vector by single-cell transcriptomics

Filippos T. Charitidis,[1] Elham Adabi,[1] Frederic B. Thalheimer,[1] Colin Clarke,[2,3] and Christian J. Buchholz[1,4]

[1]Molecular Biotechnology and Gene Therapy, Paul-Ehrlich-Institut, Paul-Ehrlich-Strasse 51–59, 63225 Langen (Hessen), Germany; [2]National Institute for Bioprocessing Research and Training, Fosters Avenue, Blackrock, A94 X099 Co. Dublin, Ireland; [3]School of Chemical and Bioprocess Engineering, University College Dublin, Belfield, D04 V1W8 Dublin, Ireland; [4]Medical Biotechnology, Paul-Ehrlich-Institut, Paul-Ehrlich-Strasse 51–59, 63225 Langen (Hessen), Germany

Quantifying gene expression in individual cells can substantially improve our understanding about complex genetically engineered cell products such as chimeric antigen receptor (CAR) T cells. Here we designed a single-cell RNA sequencing (scRNA-seq) approach to monitor the delivery of a CD19-CAR gene via lentiviral vectors (LVs), i.e., the conventional vesicular stomatitis virus (VSV)-LV and the CD8-targeted CD8-LV. LV-exposed human donor peripheral blood mononuclear cells (PBMCs) were evaluated for a panel of 400 immune response-related genes including LV-specific probes. The resulting data revealed a trimodal expression for the *CAR* and *CD8A*, demanding a careful distribution-based identification of CAR T cells and CD8+ lymphocytes in scRNA-seq analysis. The fraction of T cells expressing high *CAR* levels was in concordance with flow cytometry results. More than 97% of the cells hit by CD8-LV expressed the *CD8A* gene. Remarkably, the majority of the potential off-target cells were in fact on-target cells, resulting in a target cell selectivity of more than 99%. Beyond that, differential gene expression analysis revealed the upregulation of restriction factors in *CAR*-negative cells, thus explaining their protection from CAR gene transfer. In summary, we provide a workflow and subsetting approach for scRNA-seq enabling reliable distinction between transduced and untransduced cells during CAR T cell generation.

INTRODUCTION

In the time since Gross *et al.* generated genetically modified T cells to express a chimeric antigen receptor (CAR), many advances have been made including the development of second-generation CARs, which has led to impressive clinical benefit, particularly for patients suffering from B cell lymphoma and acute lymphoblastic leukemia (ALL), through targeting the CD19 antigen.[1-5] Further improvements, aiming at on one hand the expansion of CAR T cells to the treatment of other cancer entities including solid tumors and on the other hand the simplification of the manufacturing process, are the focus of ongoing research. Especially the complex manufacturing process, which results in a patient-specific, highly complex mixture of various T cell types, requires novel single-cell-based analysis tools to allow a better understanding and improvements.

A typical manufacturing process comprises the *ex vivo* delivery of the CD19-CAR gene into autologous T cells, subsequent CAR T cell expansion, and finally the adoptive transfer of the personalized medicinal product. Among the most frequently used gene delivery tools is the lentiviral vector (LV).[6] Carrying two positive single-stranded RNA molecules, the therapeutic gene spans between two extreme long terminal repeats (LTRs). The 5'-LTR serves as a promoter during the production of LV, transcribing the viral genomic RNA (gRNA), whereas the 3'-LTR, also known as self-inactivating LTR (SIN), contains a common polyadenylation site of both viral gRNA and the transgene's mRNA.[7] Upon cellular entry, its gRNA is reverse transcribed and the transfer cassette integrates into the host genome. Consequently, only the therapeutic gene of interest is expressed via an internal promotor.[6,8] Downstream of the therapeutic gene, the woodchuck hepatitis virus post-transcriptional regulatory element (*WPRE*) serves as an enhancing factor for increased gene expression.[9]

Viral envelope glycoproteins are responsible for the recognition and the engagement of particular host receptors, leading to particle entry. Conventional LVs are pseudotyped with vesicular stomatitis virus (VSV) glycoprotein G and accordingly enter cells through the low-density lipoprotein receptor (LDLR), which is expressed on T cells activated with anti-CD3, anti-CD28 antibodies and cultivated in the presence of cytokines.[10,11] More advanced LVs are pseudotyped with engineered glycoproteins mediating selective entry into cell types expressing a target cell surface receptor of choice.[12] For selective gene delivery into T lymphocyte subtypes, LVs with very high selectivity for CD4+ or CD8+ T cells have been described.[13] The CD8 receptor-targeted LV (CD8-LV) enables specific transduction of CD8 cytotoxic T cells, not only *ex vivo* but also *in vivo* including CAR T cell generation in humanized mice.[14,15] CAR T cell generation with LVs is a process covering

Received 23 July 2021; accepted 29 September 2021;
https://doi.org/10.1016/j.omtm.2021.09.019.

Correspondence: Christian J. Buchholz, Molecular Biotechnology and Gene Therapy, Paul-Ehrlich-Institut, Paul-Ehrlich-Strasse 51–59, 63225 Langen (Hessen), Germany.
E-mail: christian.buchholz@pei.de

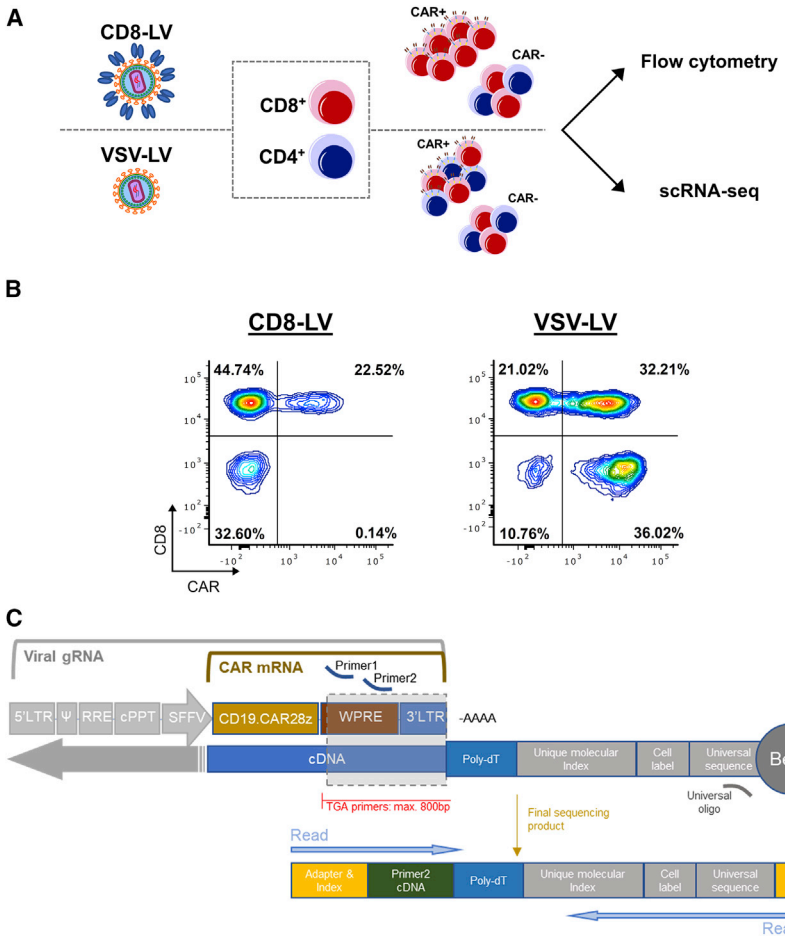

Figure 1. Methodological approach

(A) Experimental workflow. (B) Flow cytometry analysis of CAR T cells generated by CD8-LV or VSV-LV. (C) Location of customized primers (primer 1, primer 2) for amplification and subsequent detection of CAR mRNA and/or viral gRNA. Barcode elements required for cell and mRNA molecule identification are coupled with magnetic beads. After the cDNA synthesis, barcodes attach to the 3'-end of the targeted gene, enabling the matching of the paired-end reads performed by an Illumina sequencer.

~12 days. The first half includes T cell activation, incubation with vector particles, followed by vector entry and genomic integration, and finally the expression and cell surface transport of the CAR. The second half is mainly expansion of the CAR T cells to reach sufficient numbers for transplantation. The transduction process contains many unknowns on the cellular and molecular levels, such as why certain T cells become CAR-positive and others do not or what consequences the vector particle exposure has for T cells. Questions like this can now be addressed by single-cell RNA sequencing (scRNA-seq). However, as an emerging tool in the field, only a few studies have analyzed CAR T cells via scRNA-seq so far. These studies focused mainly on the diversity of CAR T cell phenotypes in pre-infusion products and correlated these to activities in patients[16-18] or investigated the consequences of different CAR signaling domains and antigenic stimulation.[19,20]

None of these studies has looked closely into the process of LV-mediated transduction. Our scope was to establish a methodology that thoroughly investigates differences between transduced and non-transduced cells during product generation and profiles the consequences of different vector types applied. We have set up a nanowell-based scRNA-seq approach for LV-mediated CAR delivery making use of the high selectivity of CD8-LV for CD8+ T cells. In particular, we have performed a targeted gene amplification analysis of untransduced CD8-LV- and VSV-LV-generated CAR T cell products expanded for a short period of time. The CAR T cells were detected via 3'-end-targeted amplification of the transgene with customized primers annealing within the *WPRE* region. This approach enabled us to accurately associate changes in cellular gene expression caused by the CAR and/or exposure to the LV particles and demonstrate that CD8-LV has near-perfect selectivity for its target cells.

RESULTS

Setting up the system

Human donor peripheral blood mononuclear cells (PBMCs) were used as the cell source for CAR T cell generation. The cells were activated and then incubated with CD8-LV or VSV-LV or left untransduced as control. After 6 days of cultivation in the presence of interleukin (IL)-7/IL-15, the cells were analyzed by flow cytometry and processed for scRNA-seq (Figure 1A). Vector doses were optimized such that a similar fraction of CD8+ CAR T cells was obtained with both vector types, while also leaving a significant fraction of cells CAR-negative (Table 1). According to flow cytometry, CD8-LV had generated 22.5% CAR T cells, all of which were CD8-positive. Thus, about one-third of the CD8 cells had been converted to CAR T cells (Figure 1B). With VSV-LV, similar fractions of CD8+ and CD4+ CAR T cells were obtained (Figure 1B). Thus, CAR T cell generation had worked out as expected. For scRNA-seq, we chose a microwell-based system for single-cell isolation and processing. Rather than utilizing a whole transcriptome approach, we opted for a targeted gene panel covering 399 human genes relevant for immune response to achieve high resolution of the sequencing results, thus allowing highly sensitive detection of differentially expressed genes. To detect CAR-positive T cells by scRNA-seq, the *WPRE* element adjacent to the 3'-LTR was identified as being at an ideal distance from the poly(A) tail to allow sensitive detection of mRNA transcribed from the integrated vector genome (Figure 1C).

Table 1. Characteristics of the applied vectors and generated CAR T cells

Sample	MOI[a]	Particles/cell	VCN[b]	Viability[c]
Untransduced	–	–	n.d.	62.7%
CD8-LV	0.045	12×10^3	0.91 ± 0.71[d]	69.3%
VSV-LV	33.3	5.8×10^3	3.94 ± 1.76	74.6%

n.d., non-detectable.
[a]As determined on MOLT cells.
[b]VCN was measured in replicates from different samples generated using different batches of LVs on three donors, including the batch and donor used in the scRNA-seq experiment (untransduced n = 3, CD8-LV n = 7, VSV-LV n = 14) (mean ± standard deviation).
[c]Determined by BD Rhapsody scanner upon staining with calcein AM and DRAQ7, before single-cell seeding.
[d]VCN was quantified on DNA extracted from whole samples and extrapolated on CD8 cells based on their frequency determined by flow cytometry.

The high selectivity of CD8-LV is confirmed by scRNA sequencing

Single-cell mRNA was isolated, reverse transcribed, and amplified with the pool of primers from the Immune Response Panel (BD Biosciences) and the customized *WPRE* primers. Quality analysis of the generated cDNA libraries was within the expected range as determined by fragment analysis (Figure S1A). Low-quality cells (185 in total), which passed the Seven Bridges pre-processing filtering steps but showed too low or too high content of targeted genes and RNA molecule numbers, were eliminated from the analysis (Figure S1B). For the initial computational analysis, post-processed samples were merged in one Seurat object and principal component analysis was conducted, choosing the first 40 components for further analysis and uniform manifold approximation and projection (UMAP) plotting (Figures S1C and S2A). Unsupervised clustering identified 14 clusters (Figure S2B). The expression of the major T cell-associated markers was analyzed across the clusters, and, subsequently, clusters were merged depending on their identity (Figure S2C). The expected cell types such as CD4, CD8, γδ T cells, and some mixed population of natural killer T (NKT) cells were present, while transduced and untransduced samples showed similar cellular compositions (Figure 2A; Figure S2D). The only exception was a small cluster of B cells in the untransduced control sample (Figure 2A; Figure S2D). Presence of residual B cells during the first days of PBMC cultivation was expected, and their absence was previously demonstrated to be due to CAR T cell-mediated killing.[14] The absence of B cells in the transduced samples thus confirmed the killing activity of the generated CAR T cells.

When we plotted normalized gene expression data for CD8A-expressing cells, a trimodal distribution of $CD8A^{high}$, $CD8A^{low}$, and cells with undetectable or absent *CD8A* mRNA ($CD8A^{neg}$ cells) became obvious in all samples (Figure 2B). Performing multimodal analysis, we identified the peaks of the modes as well as the antimodes, which we used as thresholds for gating of the populations (Figure S3). For the $CD8A^{high}$ cells, this resulted in the most confined population of CD8 cells in UMAP plots (Figure 2B). On the other hand, $CD8A^{low}$ and $CD8A^{neg}$ cells comprised the rest of immune cell populations, including CD4 cells. While less pronounced, a similar tendency for a trimodal distribution was also observed for CAR T cells as determined by the CAR transgene expression (Figure 2B; Figure S3).

Next, we compared these data to the flow cytometry results generated from identical cell samples. Interestingly, we observed concordant CAR T cell frequencies between flow cytometry and scRNA data when we subset for CAR^{high} and $CD8A^{high}$ in the scRNA plots. Then, 23.2% CAR T cells were identified by scRNA with CD8-LV (Figure 2C). Notably, our subsetting approach showed that 97.5% of CAR^{high} cells were $CD8A^{high}$ cells in the CD8-LV sample (Figure 2D) and 2.5% of CAR^{high} cells (in total 59 cells) were $CD8A^{neg/low}$. These potential off-target cells consisted of 54.2% γδ T cells, 6.8% CD4/CD8 double-positive cells, 3.4% NKT cells, and 25.4% CD4 cells (Table 2; Figure S4). Of all these, only 28.8% were $CD8A^{neg}$ and $CD8B^{neg}$ double-negative cells (Table 2). Importantly, a close match in the frequencies of CD8 and CD4 CAR T cells between flow cytometry and scRNA analysis was also observed for CAR T cells generated with VSV-LV (Figure 2C), which nicely validated our gating strategy.

The CAR^{low}-expressing cells consisted of all identified immune cells, including CD8, CD4, γδ T, and NKT cells (Figures 2A and 2B). Comparison of their expression profile with that of CAR^{neg} cells revealed no significant differences between these two cell populations, whereas significant differences were obvious between CAR^{low} and CAR^{high} cells (Figure S5). We therefore combined them with the CAR^{neg} cells in one group ($CAR^{neg/low}$) for further analysis. Notably, CAR^{low} cells were substantially different from untransduced cells, which had not been exposed to vector particles (Figures S5A and S5B).

Differentially expressed genes in the CD8+ populations

By analyzing the isolated cell subsets of CD8 T cells, as described above, we observed alterations of gene expression profiles across the populations. The differentially expressed genes for each group identified by expression analysis are shown in the heatmap plot in Figure 3A. Intriguingly, we observed differences between the $CAR^{neg/low}$ cells from the two vector types (Figure 3A). Moreover, we also observed significant differences in 58 genes between the CAR^{high} populations transduced by the two LVs (Figure 3A; Figure S6). Disregarding the LV type used for transduction, biggest differences were observed between untransduced (cells that were never exposed to LVs) and $CAR^{neg/low}$ cells (LV-exposed cells) and also between untransduced and CAR^{high} cells, whereas the fold-change gene expression difference between $CAR^{neg/low}$ and CAR^{high} cells was clearly less pronounced (Figure 3B). When comparing the particular vector types among each other or against untransduced, the differences from untransduced were in each case more pronounced, in terms of both the number of genes and the fold change, than the difference between CD8-LV- and VSV-LV-exposed cells (Figure 3B).

The majority of the differentially expressed genes, 130 out of 151 either up- or downregulated, were identified when comparing untransduced with CAR^{high} cells (Figure 3C, left). From these, 70 genes

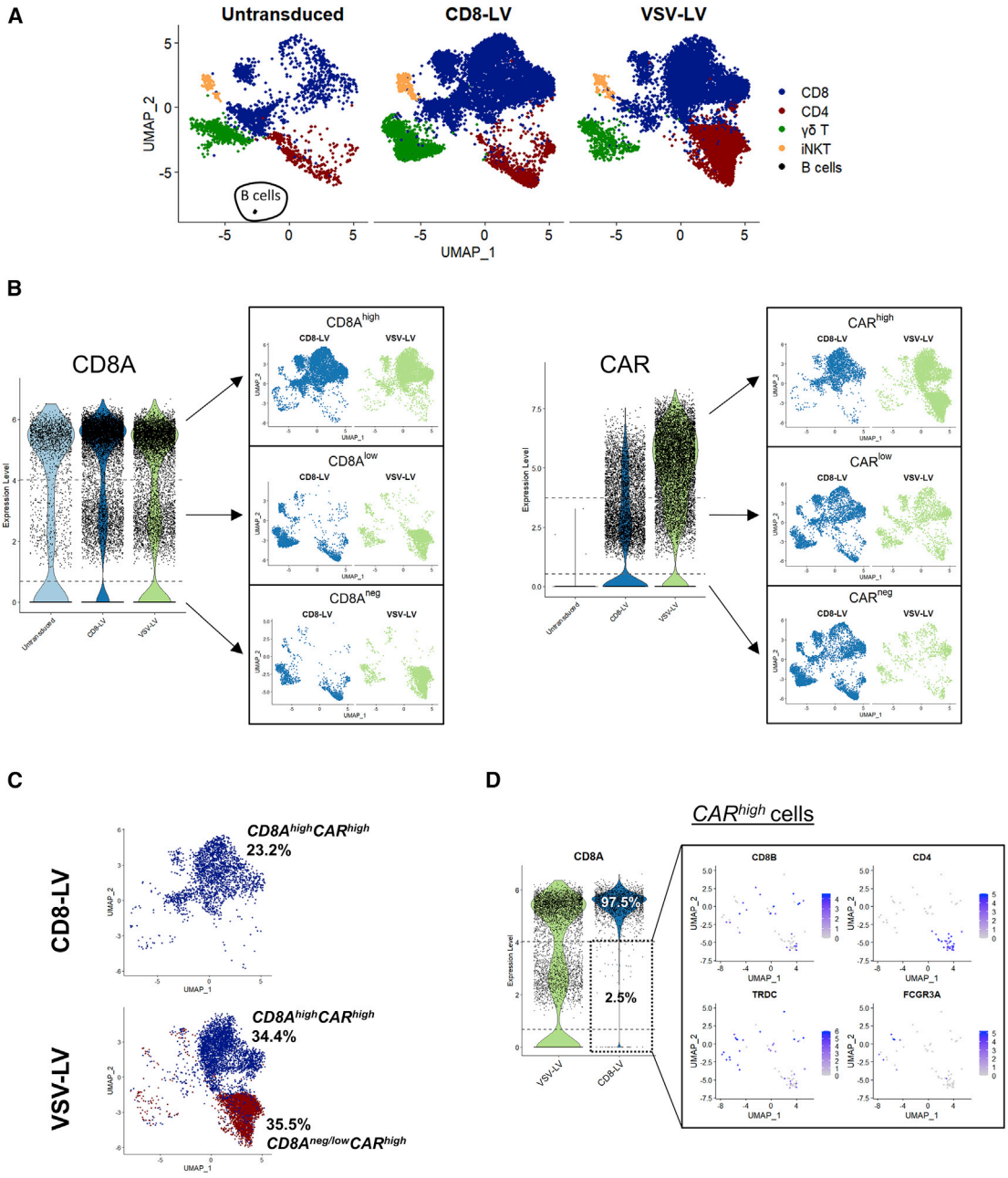

Figure 2. CAR gene expression and CAR T cell subpopulations

(A) UMAP plots of the three samples colored for the major immune cell subtypes identified by the expression of marker genes. (B) Subsetting strategy based on the distribution of highly, low, and negatively expressing cells for *CD8A* and *CAR* genes and their projection into UMAP plots for cell population and purity evaluation. (C) Frequency of CAR T cells identified in scRNA sequencing based on the multimodal subsetting strategy. (D) *CD8A* expression of CAR^{high} cells across LV-exposed samples (left). Analysis of $CD8A^{neg/low}/CAR^{high}$ cells identified in the CD8-LV sample for the expression of CD8, CD4, and TCRγδ.

were shared between the comparisons of untransduced with either CAR^{high} or $CAR^{neg/low}$ cells, 33 genes were shared in all of the comparisons, including $CAR^{neg/low}$ with CAR^{high}, whereas 43 were unique, comprising the biggest difference in that group of comparison. On the other hand, by comparing the whole CD8 cell groups between control and CD8-LV or VSV-LV, we found that most of the differentially expressed genes were shared between the vectors, when comparing control with transduced samples (100 out of 149), whereas 29 genes were commonly identified in all of the three comparisons (Figure 3C, right). Gene set enrichment analysis with the Gene

Table 2. Identification of $CAR^{high}CD8A^{neg/low}$ cells after CD8-LV mediated transduction

Cell type	Marker genes	Cell number
CD4 T cells	$CD4^{pos}CD8B^{neg}$	**15**
	$CD8A^{low}$	7
	$CD8A^{neg}$	8
CD8 T cells	$CD8B^{pos}$	**5**
	$CD8A^{low}$	5
CD4/CD8 T cells	$CD4^{pos}CD8B^{pos}$	**4**
	$CD8A^{low}$	2
	$CD8A^{neg}$	2
NKT	$FCGR3A^{pos}$	**2**
	$CD8B^{pos}CD8A^{low}$	1
	$CD8B^{neg}CD8A^{low}$	1
γδ T	$TRDC^{pos}$	**32**
	$CD8B^{pos}CD8A^{low}$	7
	$CD8B^{pos}CD8A^{neg}$	7
	$CD8B^{neg}CD8A^{low}$	9
	$CD8B^{neg}CD8A^{neg}$	9
Remaining cells	$CD8B^{neg}CD4^{neg}TRDC^{neg}FCGR3A^{neg}$	**1**
	$CD8A^{low}$	1

Numbers in bold indicate total counts of the subfractions listed below, respectively.

Ontology (GO) Biological Process database revealed enrichment of genes especially related with cytokine-mediated signaling, T cell activation and immune response, and regulation of cell proliferation or apoptosis (Figure S7).

Looking closer into particular genes of CD8+ cells that show a significant level of up- or downmodulation between the different settings, we grouped them into topics related to CAR activities and vector-host interactions (Figure 4). With respect to T cell activation, upregulation of *CD70*, *ICOS*, and *JUNB* (part of the AP-1 transcription factor) selectively in the CAR^{high} cells is most likely a result of the CAR-mediated activities (Figure 4A). CAR^{high} CD8 cells favored a TH1-phenotype as exemplified by upregulated IL-12 receptor (*IL12RB2*) (Figure 4B) and granulocyte-macrophage colony-stimulating factor (GM-CSF) (*CSF2*) (Figure 4C) as well as an unaltered expression of interferon-γ (*IFNG*) and *STAT4* (Figure S8). Unchanged expression of *TNF* (Figure S8) and reduced levels of *FAS* (Figure 4D), which can trigger both T cell apoptosis as well as increased levels of *IER3*, are well in line with an anti-apoptotic profile in CAR^{high} cells (Figure 4D).[21] The expression of several exhaustion and immune checkpoint markers (*ENTPD1*, *LAG3*, *HAVCR2*, *LAT2*, *CTLA4*) (Figure 4E) accompanied by the increase in co-stimulatory markers (*ICOS, CD70, CD27*) (Figure 4A) indicated early exhaustion of the CAR^{high} CD8 cells, potentially as a result of CAR tonic signaling.[22] Finally, we found the mitogen-activated protein (MAP) kinase phosphatase-2 (*DUSP4*), which is known to inactivate MAP and extracellular signal-regulated kinase (ERK) kinases as well to promote TH1 response, to be significantly upregulated in CAR^{high} cells (Figure 4F).[23,24]

Besides being caused by CAR activities, differences between $CAR^{neg/low}$ and CAR^{high} cells may have been caused by intrinsic factors present in particular cells preventing proper transduction by the LVs. Among these is the IL-2 receptor alpha subunit (*IL2RA*), which we found to be downmodulated in the $CAR^{neg/low}$ cells not only compared to CAR^{high} cells but also compared to untransduced cells (Figure 4A), suggesting that their low activation level contributed to being protected from gene transfer. In line with this, *PIK3IPI* implicated in inhibition of T cell activation was upregulated in the $CAR^{neg/low}$ population (Figure 4A), further confirming the low activation status of these cells.[25] Although only slightly upregulated, both interferon-induced transmembrane proteins covered by the panel, *IFITM2* and *IFITM3*, were significantly higher in $CAR^{neg/low}$ cells than in untransduced or CAR^{high} cells (Figure 4F).

Besides changes in gene expression in the CAR^{high} cells only, we identified several genes that were up- or downregulated in both CAR^{high} and $CAR^{neg/low}$ cells compared with untransduced cells. Thus, these changes were most likely due to the exposure to LV vectors. This referred to the negative regulators of proliferation and inhibitors of T cell activation *CD37* and *PIK3IPI*, respectively (Figure 4A),[25,26] as well as co-stimulatory and phenotype markers such as *CD27*, *CD7*, *CD62L (SELL)*, and *TCF7* (Figures 4A and 4G). Typical markers for apoptosis induction (*CASP5*) (Figure 4D) and exhaustion (*LIF*, *C10orf54*) (Figure 4E) were also induced upon exposure to LV particles. Of particular interest in this context are antiviral response factors. Indeed, *BTG1*, a cell cycle regulator,[27] the CD11c gene (*ITGAX)*, *IFITM3*, and in part also *IRF4* were all upregulated upon exposure to LVs (Figures 4F and 4H).

Finally, gene profile variations were observed between the samples exposed to the two different LVs. In particular, *ITGAX* (Figure 4F) as well as the cytotoxic cytokine TRAIL gene (*TNFSF10*) (Figure 4I), *CCR7*, and *CD62L* (*SELL*) (Figure 4G) exhibited a tendency to be more upregulated in cells that had been exposed to VSV-LV than in those exposed to CD8-LV. On the other hand, the lysosomal enzyme lipase A (*LIPA*) was found to be more downmodulated in the VSV-LV sample (Figure 4H). Further examples for differences between these two groups referred to cathepsin D (*CTSD*) (Figure 4H), the chemokines *CCL3* and *CCL4* (Figure 4C), and granulysin (*GNLY*) (Figure 4I), which were selectively upregulated in CD8-LV-exposed cells.

DISCUSSION

Deploying single-cell analysis tools in CAR T cell therapy can potentially not only improve the development and the optimization of the upstream processes but also enhance the clinical efficacy and reduce post-transfusion side effects by neutralizing product variations. In particular, failures in the subsetting of the exact CAR T cell population due to improper distinction between transduced and non-transduced cells can have immediate consequences for any biological

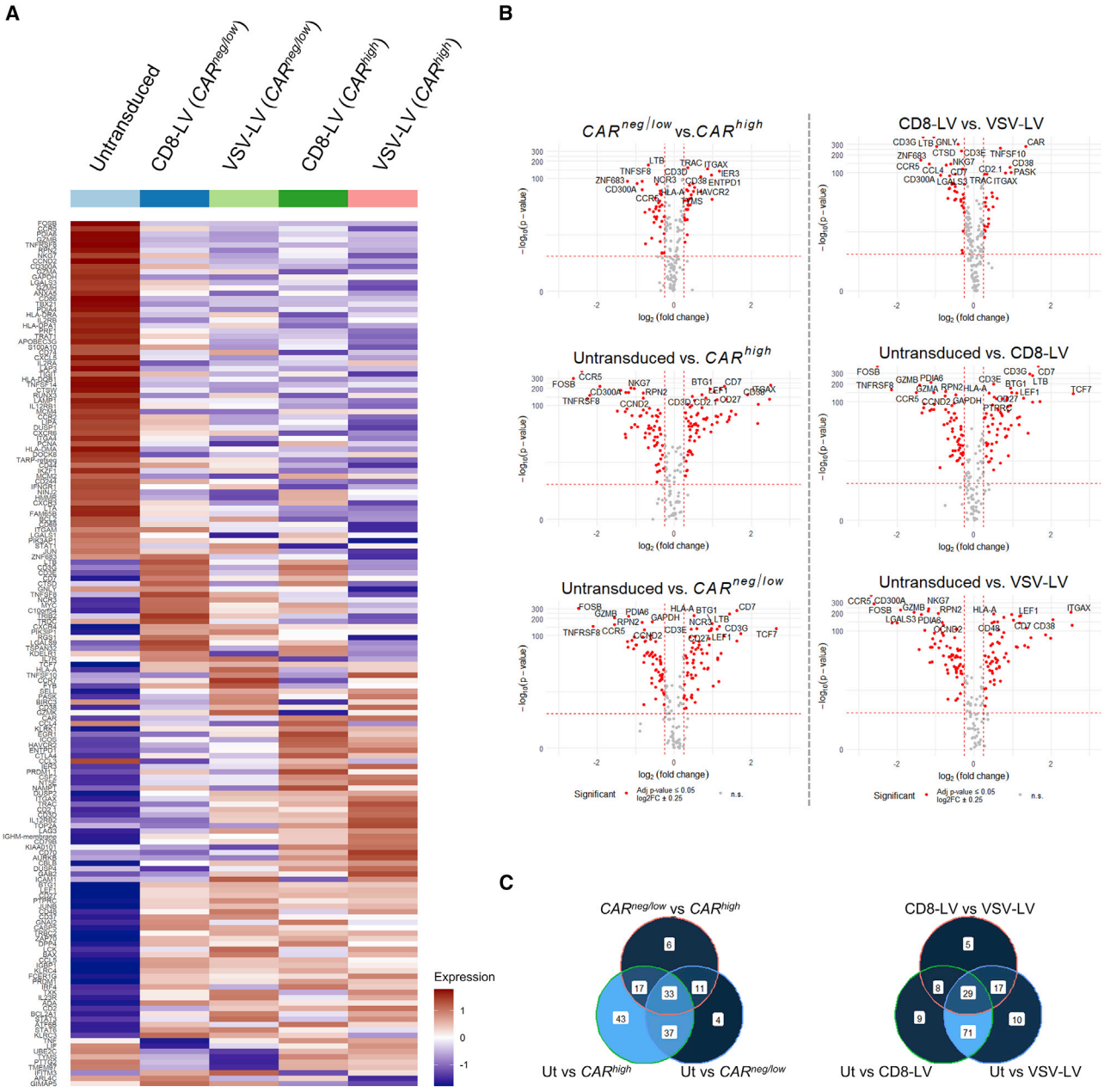

Figure 3. Differentially expressed genes in the subpopulations

(A) Heatmap plots of 161 significantly differentially regulated genes identified for all groups compared (untransduced n = 1,444; CD8-LV [$CAR^{neg/low}$] n = 4,216; VSV-LV [$CAR^{neg/low}$] n = 1,739; CD8-LV [CAR^{high}] n = 2,257; VSV-LV [CAR^{high}] n = 3,084) by the FindAllMarkers function in Seurat (log_2(fold change) ± 0.25, adjusted p value < 0.05). (B) Volcano plots comparing CAR^{high}, $CAR^{neg/low}$, and untransduced (Ut) cells, disregarding the LV used (left) and comparisons of the CD8+ populations in the CD8-LV, VSV-LV, and Ut samples (right). The fold change of CAR is not shown in every plot due to $log_2FC > 3$. (C) Overlaps of differentially expressed genes identified based on CAR expression levels (left) and vector types (right).

conclusions drawn from the data. In this study, we have therefore started to follow early time points in CAR T cell generation, especially focusing on the transduction process with the final goal to improve the identification of the various subpopulations and to better understand why particular cells are becoming CAR T cells and others not. Key for our analysis was the use of CD8-LV, which is known to be highly selective for the CD8+ T cells in human PBMCs.[15] This facilitated identification of the transduced CD8+ T cells and their comparison to CAR T cells generated with the conventional VSV-LV. We decided to perform a targeted gene amplification and sequencing

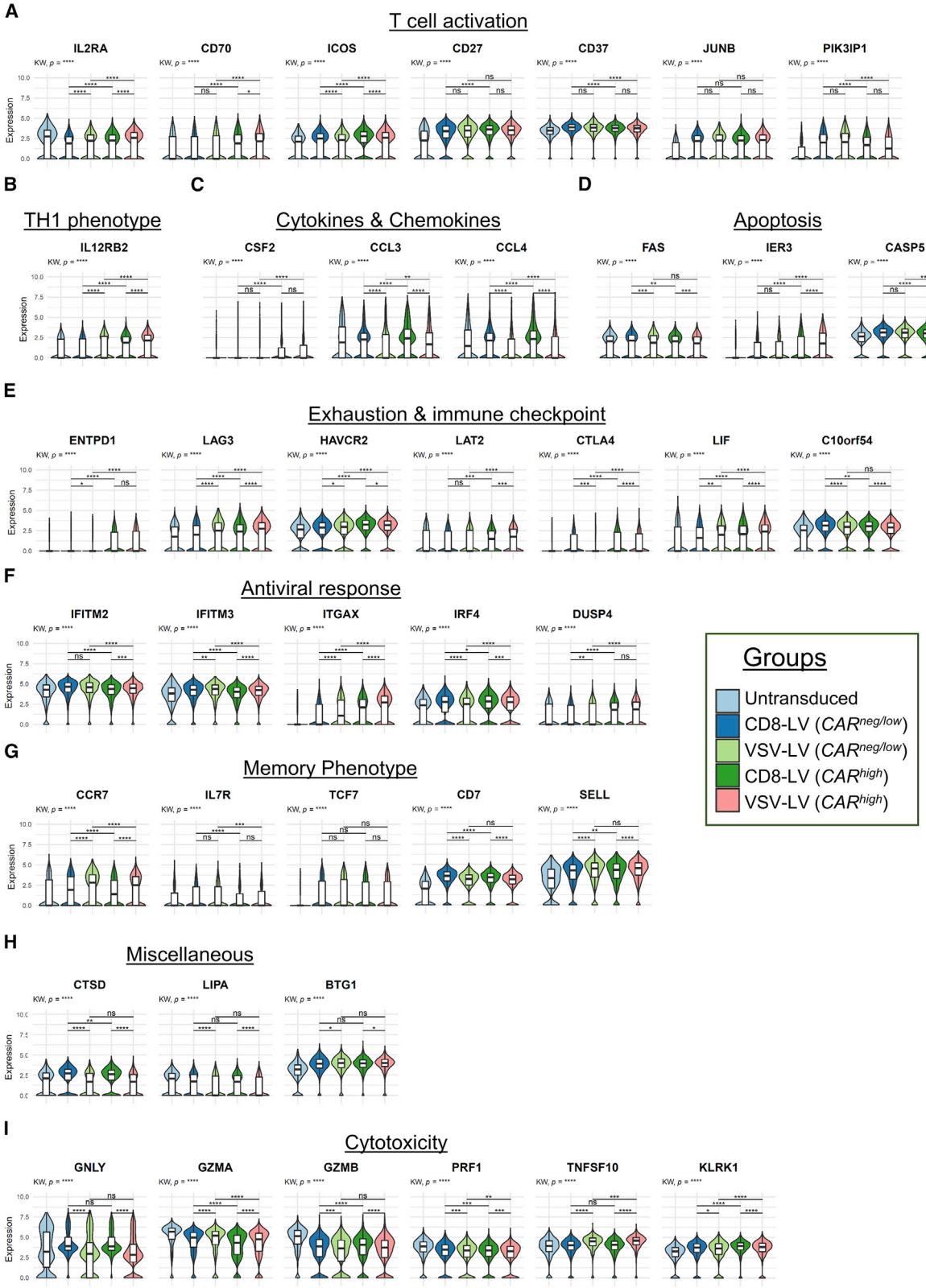

(legend on next page)

analysis covering ~400 genes to establish our methodological approach. In particular, comparing to a typical whole transcriptome experiment requiring 50,000 reads/cell, we managed to efficiently sequence with ~4,000 reads/cell without compromising the sequencing saturation and depth.[28] This allowed us to increase the processed cell number by up to 10-fold compared to a typical whole transcriptome analysis (WTA) run and yet have a high resolution of the expressed genes.

Our approach identified a trimodal distribution not only in the expression of the *CAR* gene but also for *CD8A*. Notably, previous studies have not described this.[16-20] Since the expression profiles of CAR^{low} and CAR^{neg} cells were basically identical, they were merged for the downstream analyses (Figure S2A). The situation appears more complicated with the $CD8A^{low}$ population. Indeed, the PBMCs used in this study include besides T lymphocytes also natural killer (NK) cells and dendritic cells (DCs). However, almost all $CD8A^{low}$ cells were CD3+, thus rather excluding the presence of NK cells and DCs as explanation (Figure S2D). Instead, it is likely that transient fluctuations in mRNA levels that do not immediately convert in loss of the encoded proteins have accounted for this.[29]

In the current study, we have evaluated the selectivity of a receptor-targeted vector by both flow cytometry and scRNA-seq, thus on protein and mRNA levels. The obtained data on one hand were in perfect agreement with flow cytometry-based selectivity analysis and on the other hand confirmed the high, near-absolute selectivity of CD8-LV for its target cells (Figures 1B and 2D). Of the 59 (2.5%) potential off-target cells, 9 were in fact CD8+ or double-positive cells based on the expression of *CD8B*. Of the remaining 50 cells, 32 were γδ T cells, of which only 9 express neither *CD8A* nor *CD8B*; 2 cells were NKT cells; 15 were CD4 cells, of which 8 were negative for CD8 markers whereas 7 had $CD8A^{low}$ expression (Table 2). This leaves just 17 cells that could be true off-target cells and thus an on-target rate of 99.28%. However, even these few cells could be target cells when considering the above-mentioned mRNA fluctuation. Combining barcoded antibody staining with expression profiling could be a straightforward next step to clarify this issue.

Our study revealed interesting differences in expression of particular genes between the groups. The data revealed transcriptomic alterations upon exposure to vector particles and expression of the CAR as the result of proper gene delivery and transduction. Thus, the exposure of cells to any of the two LVs resulted in alterations of their gene expression profiles, regardless of whether the cells were eventually properly transduced by the vector or not. These findings suggest that under the given experimental conditions exposure of T cells to LV particles results in stronger gene expression profile alterations than presence of the CAR. While CD8+ CAR^{high} cells exhibited an activated TH1 phenotype and an overall profile well in accordance with that observed in previous studies (Figure 4),[16,17,20] CD8 $CAR^{neg/low}$ cells expressed genes that potentially restricted cell viability, phenotype, and viral entry. These cells had upregulated genes involved in inhibition of T cell activation (*PIK3IP1*) and proliferation (*CD37, BTG1*) as well as promoting pyroptosis (*CASP5*), a type of programmed cell death resulting in inflammatory cytokine release (Figures 4A, 4D, and 4H).[25,26,30,31] Particularly remarkable was the observation that two restriction factors (*IFITM2, IFITM3*) directly implicated in preventing viral entry were significantly increased in those cells that remained CAR^{neg} despite having been exposed to LVs (Figure 4F). The two interferon-induced transmembrane proteins expressed from *IFITM2* and *IFITM3* reside in endosomal compartments and inhibit the fusion of the viral envelope with the endosomal membrane, a process characteristic for the pH-dependent entry pathway of VSV-LV.[32] *IFITM3* has been investigated most and was recently identified as the main target to improve gene transfer into hematopoietic stem cells through the use of resveratrol as transduction enhancer.[33-35] Although our data certainly support this strategy also for T lymphocytes, they also suggest that not only intracellular localization of IFITMs but also subtle changes in their overall expression levels may determine whether a particular T cell becomes properly transduced.[35]

Differences in gene profiles between the cells exposed to CD8-LV versus VSV-LV were also observed, although we previously demonstrated that CAR T cells generated with each of the two vector types were equally active in killing tumor target cells.[15] These might be a consequence of the viral entry pathway used, toxicity of VSV-LV or the transduction of CD4 cells by VSV-LV thus affecting CD8 cells in a paracrine cytokine secretion-driven manner. *CCL4* (MIP-1β), a major HIV suppressive factor, was highly upregulated in CD8 cells of the CD8-LV sample, indicating a possible antiviral response against the Nipah virus-derived envelope of CD8-LV (Figure 4C).[36] In addition, CCR7 and CD62L were upregulated upon VSV-LV exposure, indicating a more pronounced central memory phenotype in these CAR T cells than in those generated with CD8-LV (Figure 4G). This is in line with granulysin (*GNLY*) increase in the CD8-LV sample, which is indicative for a more cytotoxic activity of these CAR T cells (Figure 4I).[37] Although a central memory phenotype is beneficial for CAR T cell persistence,[38] previous phenotype comparisons between CAR T cells generated with VSV-LV versus CD8-LV did not reveal significant differences.[15] In the same direction, cathepsin-D peptidase (*CTSD*) was significantly increased in the CD8-LV sample (Figure 4H). It prevents oxidative stress-induced cell death, a feature relevant for CD3/CD28-activated T cells, in which the glycolysis pathway is elevated because of a skew to effector

Figure 4. Violin plots for genes of interest

Representative differentially expressed genes in CD8+ subpopulations clustered into topics related to CAR activities and vector-host interactions. (A) T cell activation. (B) TH1 phenotype. (C) Cytokines and chemokines. (D) Apoptosis. (E) Exhaustion and immune checkpoint. (F) Antiviral response. (G) Memory phenotype. (H) Miscellaneous. (I) Cytotoxicity. KW, Kruskal-Wallis multiple comparison test. Wilcoxon rank-sum test performed for pairwise comparisons. p values adjusted based on Bonferroni; ns, non-significant; *$p < 0.05$, **$p < 0.01$, ***$p < 0.001$, ****$p < 0.0001$. The bars in box plots indicate the 25th to 75th percentile range and the median value is shown with a horizontal line.

phenotype leading to production of reactive oxygen species (ROS).[39,40] In the VSV-LV sample, a lysosomal lipase (*LIPA*) was downregulated, which correlates with the endosomal-related pH-dependent entry pathway of VSV-LV (Figure 4H).

Although further investigation will be required before final conclusions on up- or downregulation of particular genes can be drawn, we have here successfully established a scRNA-seq workflow for CAR T cells, generated with conventional or receptor-targeted LV, and managed to distinguish transduced from untransduced cells by implementing a customized pair of primers. Based on the distribution of gene expression, we propose a subsetting method for distinguishing CAR T cells in scRNA-seq analysis, wherever applicable.

MATERIALS AND METHODS

Cell culture

HEK293T (ATCC CRL-11268) cells were cultured in Dulbecco's modified Eagle's medium (DMEM) (Sigma-Aldrich, Munich, Germany) supplemented with 2 mM glutamine (Sigma-Aldrich) and 10% fetal calf serum (FCS) (Biochrom, Berlin, Germany). MOLT 4.8 cells were cultured in RPMI 1640 (Biowest, Nuaillé, France) supplemented with 10% FCS and 2 mM glutamine. All cell cultures were incubated at 37°C with 5% CO_2 and 90% humidity.

Generation of lentiviral vectors

A detailed protocol describing the generation of T cell-targeted LVs was recently published.[41] In brief, second-generation LVs were produced as previously described by co-transfecting 2×10^7 HEK293T cells per T125 flask with a plasmid cassette, consisting of packaging plasmid (pCMVΔR8.9) and transfer plasmid (pSEW-mycCD19-CAR-28z), in the presence of linear polyethylenimine (PEI). For the generation of VSV-pseudotyped LV we co-transfected the plasmid encoding the envelope G-glycoprotein (pMD2.G) and for the CD8-LV the plasmids encoding the mutated G-glycoprotein of the Nipah virus coupled with single-chain anti-CD8α (pCAGGS-NiV-Gd34-CD8) and the truncated fusion glycoprotein (pCAGGS-NiV-Fd22). LVs were harvested from culture supernatants, concentrated by a 24-h centrifugation through a 20% sucrose cushion at 4,500 × *g* (4°C), and re-suspended in 60 μL per flask Dulbecco's phosphate-buffered saline (DPBS, Mg^{2+} and Ca^{2+} free), followed by aliquoting and freezing at −80°C. LVs were thawed only once for each experimental use.

Transduction units per mL (TU/mL) were calculated based on the titration of the vector stocks on MOLT 4.8 cells. The multiplicity of infection (MOI) applied in each experimental condition was calculated by correlating the transducing units added to the number of cells present in the PBMC culture. Particle numbers in the vector stocks were measured by nanoparticle tracking analysis using the NanoSight device as previously described.[12]

PBMC isolation, culture, and transduction

PBMCs were purified from a buffy coat derived from an anonymous donation collected at the German Red Cross blood donation center (DRK-Blutspendedienst Baden-Württemberg-Hessen, Frankfurt) by Pancoll (PAN-Biotech, Aidenbach, Germany) density gradient centrifugation and cryopreserved in 90% FCS and 10% dimethyl sulfoxide (DMSO). Cells were thawed at 37°C, washed, and activated for 72 h in a 6-well plate with pre-coated human recombinant anti-CD3 (1 μg/mL, clone OKT3, Miltenyi Biotec, Bergisch Gladbach, Germany), soluble anti-CD28 (3 μg/mL, clone 15E8, Miltenyi Biotec), supplemented with the cytokines IL-7 (25 IU/mL) and IL-15 (50 IU/mL), in RPMI medium with 10% FCS, 2 mM glutamine, 0.5% penicillin-streptomycin, and 25 mM *N*-2-hydroxyethylpiperazine-*N*′-2-ethanesulfonic acid (HEPES) (Sigma-Aldrich). After activation, 8×10^4 cells per well were seeded in a 96-well plate and spinoculated with 1 μL of each LV stock at 850 × *g* and 32°C for 90 min. Medium was refreshed once after 72 h of inoculation. Final samples were collected and processed 6 days post-inoculation.

For quantification of the vector copy number (VCN), genomic DNA was isolated from at least 2.5×10^5 cells with the DNeasy blood and tissue kit (QIAGEN, Hilden, Germany) according to the manufacturer's instructions, after elution with DNA-free water (Sigma-Aldrich). Real-time PCR was performed as previously described,[42] with primer pairs specific for *WPRE* and human albumin (*ALB*). VCN was calculated by the formula $(WPRE\ \text{copies})/(ALB\ \text{copies} \div 2)$. The efficiency of the standard curves was within a range of 90%–110%.

Flow cytometry

Cells were re-suspended, washed with buffer (PBS, 5% FCS, 2 mM NaN_3), and stained for 30 min at 4°C with the antibodies anti-CD3 [fluorescein] (clone BW264/56, Miltenyi Biotec), anti-CD8 [VioBlue] (clone BW135/80, Miltenyi Biotec), and anti-c-*myc* [phycoerythrin] (9B11, Cell Signaling Technology, Danvers, MA, USA) and with a fixable viability dye (eFluor 780, Thermo Fisher Scientific, Waltham, MA, USA). After staining, cells were washed twice, fixed with 0.5% paraformaldehyde (PFA), and run in MACSQuant X (Miltenyi Biotec). Results were analyzed in FCS Express v.6 (De Novo Software, Pasadena, CA, USA).

Single-cell RNA isolation, library preparation, and sequencing

Single-cell isolation and mRNA processing were conducted with the BD Rhapsody platform (BD Biosciences) according to the manufacturer's instructions (Doc IDs: 214062 and 210968, BD Biosciences). For viability evaluation, cell suspensions were incubated for 5 min at 37°C with 10 μM calcein AM (Thermo Fisher Scientific) and 1.5 μM DRAQ7 (BD Biosciences). Single cells were then captured in nanowell-containing cartridges; cellular mRNA was released after lysis and captured by poly(dT)-coated magnetic beads. Beads were subsampled to yield ∼31,000 total cells.

Reverse-transcribed cDNA was amplified with the Immune Response Panel (cat. 633750, BD Biosciences) of primers covering 399 genes. For detection of mRNA derived from the *CAR* gene in CAR T cells, we *in silico* predicted and confirmed by sequencing the poly(A) signal site within the 3'-SIN-LTR) of the transfer vector plasmid (Poly(A) Signal Miner).[43] Primers binding within 800 bp away from the poly(A) signal, thus within the *WPRE*, were then customized by BD

Biosciences (Franklin Lakes, NJ, USA) and added to the Immune Response Panel.

Libraries were indexed uniquely, and their quality and final length were assessed with the high-sensitivity NGS kit with the Fragment Analyzer (Agilent, Santa Clara, CA, USA). Data were analyzed in ProSize 2.0 (Advanced Analytical Technologies, Heidelberg, Germany) (Figure S1A). Libraries were then quantified by Qubit dsDNA HS Assay Kit (Thermo Fisher Scientific), pooled in a ratio defined by the cell number of each sample and the required sequencing depth, and loaded into a NextSeq High Output flowcell at 1 pM, spiked with 20% PhiX, and sequenced in NextSeq 550 (Illumina, San Diego, CA, USA).

Data analysis

The raw FASTQ files were processed with the bioinformatics pipeline of Seven Bridges Genomics (Charlestown, MA, USA). Overall, 21,527 cells passed the pre-processing step with a mean sequencing depth of 4,304 reads per cell. Recursive substitution error correction (RSEC)-adjusted molecule count matrices were generated and processed in R (v.4.0.3) with Seurat.[44] Thresholds for filtering the low quality of cells and the number of principal components chosen for the UMAP analysis are shown in Figures S1B–S1D. The filtering metrics as well as the final number of putative cells per sample are listed in Table S1. Wilcoxon rank-sum test for differential gene expression analysis was performed with the FindAllMarkers and FindMarkers functions, applying the thresholds of $\log_2$(fold change) ± 0.25 and minimum fraction of expressing cells 25%. Violin plots were constructed with ggplot2 (v.3.3.3), and Kruskal-Wallis non-parametric test and Wilcoxon rank-sum pairwise test were performed with rstatix (v.0.7.0).[45] GO Biological Process enrichment analysis on differentially expressed genes was performed with the Independent Enrichment Analysis tool of Appyters collection by defining the genes of the Immune Response Panel.[46] For every multiple comparison, including the differential gene expression analysis and volcano plotting, p values were corrected based on Bonferroni. Multimodal analysis was conducted with the package multimode.[47] Abbreviations used represent the following values: ns = non-significant, *p< 0.05, **p < 0.01, ***p < 0.001, ****p < 0.0001.

Data availability

The data discussed in this publication have been deposited in NCBI's Gene Expression Omnibus (GEO) and are accessible through GEO Series accession number GSE184895 (https://www.ncbi.nlm.nih.gov/geo/query/acc.cgi?acc=GSE184895).[48]

SUPPLEMENTAL INFORMATION

Supplemental information can be found online at https://doi.org/10.1016/j.omtm.2021.09.019.

ACKNOWLEDGMENTS

The authors are grateful to Csaba Miskey (Paul-Ehrlich-Institut) for his advice on library generation and sequencing, to Manuela Gallet and Vanessa Riechert (both Paul-Ehrlich-Institut) for the qPCR, as well as to Vadir Lopez-Salmeron, Edyta Kowalczyk, and Siobhan Cashman (all BD Biosciences) for their advice on the Rhapsody system. This project has received funding to C.C. and C.J.B. from the European Union's Horizon 2020 research and innovation program STACCATO under the Marie Skłodowska-Curie grant agreement No. 813453.

AUTHOR CONTRIBUTIONS

Conceptualization: C.J.B., F.T.C., and F.B.T. Data curation: F.T.C. Formal analysis: F.T.C. and E.A. Funding acquisition: C.J.B. and C.C. Investigation: F.T.C. and E.A. Methodology: C.J.B., F.T.C., and F.B.T. Project administration: C.J.B. Resources: C.J.B. and C.C. Supervision: C.J.B. Visualization: F.T.C. and E.A. Writing – original draft: F.T.C., E.A., and C.J.B. Writing – review & editing: C.J.B. and C.C.

DECLARATION OF INTERESTS

C.J.B. is listed as co-inventor of the patent for the CD8-targeted lentiviral vector. All the other authors declare no competing interests.

REFERENCES

1. Brentjens, R.J., Davila, M.L., Riviere, I., Park, J., Wang, X., Cowell, L.G., Bartido, S., Stefanski, J., Taylor, C., Olszewska, M., et al. (2013). CD19-targeted T cells rapidly induce molecular remissions in adults with chemotherapy-refractory acute lymphoblastic leukemia. Sci. Transl. Med. *5*, 177ra38.

2. Maher, J., Brentjens, R.J., Gunset, G., Rivière, I., and Sadelain, M. (2002). Human T-lymphocyte cytotoxicity and proliferation directed by a single chimeric TCRzeta /CD28 receptor. Nat. Biotechnol. *20*, 70–75.

3. Gross, G., Gorochov, G., Waks, T., and Eshhar, Z. (1989). Generation of effector T cells expressing chimeric T cell receptor with antibody type-specificity. Transplant. Proc. *21*, 127–130.

4. Schuster, S.J., Svoboda, J., Chong, E.A., Nasta, S.D., Mato, A.R., Anak, Ö., Brogdon, J.L., Pruteanu-Malinici, I., Bhoj, V., Landsburg, D., et al. (2017). Chimeric Antigen Receptor T Cells in Refractory B-Cell Lymphomas. N. Engl. J. Med. *377*, 2545–2554.

5. Maude, S.L., Laetsch, T.W., Buechner, J., Rives, S., Boyer, M., Bittencourt, H., Bader, P., Verneris, M.R., Stefanski, H.E., Myers, G.D., et al. (2018). Tisagenlecleucel in Children and Young Adults with B-Cell Lymphoblastic Leukemia. N. Engl. J. Med. *378*, 439–448.

6. Milone, M.C., and O'Doherty, U. (2018). Clinical use of lentiviral vectors. Leukemia *32*, 1529–1541.

7. Dull, T., Zufferey, R., Kelly, M., Mandel, R.J., Nguyen, M., Trono, D., and Naldini, L. (1998). A third-generation lentivirus vector with a conditional packaging system. J. Virol. *72*, 8463–8471.

8. Zaiss, A.-K., Son, S., and Chang, L.-J. (2002). RNA 3' readthrough of oncoretrovirus and lentivirus: implications for vector safety and efficacy. J. Virol. *76*, 7209–7219.

9. Zufferey, R., Donello, J.E., Trono, D., and Hope, T.J. (1999). Woodchuck hepatitis virus posttranscriptional regulatory element enhances expression of transgenes delivered by retroviral vectors. J. Virol. *73*, 2886–2892.

10. Finkelshtein, D., Werman, A., Novick, D., Barak, S., and Rubinstein, M. (2013). LDL receptor and its family members serve as the cellular receptors for vesicular stomatitis virus. Proc. Natl. Acad. Sci. USA *110*, 7306–7311.

11. Amirache, F., Lévy, C., Costa, C., Mangeot, P.E., Torbett, B.E., Wang, C.X., Nègre, D., Cosset, F.L., and Verhoeyen, E. (2014). Mystery solved: VSV-G-LVs do not allow efficient gene transfer into unstimulated T cells, B cells, and HSCs because they lack the LDL receptor. Blood *123*, 1422–1424.

12. Friedel, T., Hanisch, L.J., Muth, A., Honegger, A., Abken, H., Plückthun, A., Buchholz, C.J., and Schneider, I.C. (2015). Receptor-targeted lentiviral vectors are exceptionally sensitive toward the biophysical properties of the displayed single-chain Fv. Protein Eng. Des. Sel. *28*, 93–106.

13. Frank, A.M., and Buchholz, C.J. (2018). Surface-Engineered Lentiviral Vectors for Selective Gene Transfer into Subtypes of Lymphocytes. Mol. Ther. Methods Clin. Dev. *12*, 19–31.

14. Pfeiffer, A., Thalheimer, F.B., Hartmann, S., Frank, A.M., Bender, R.R., Danisch, S., Costa, C., Wels, W.S., Modlich, U., Stripecke, R., et al. (2018). *In vivo* generation of human CD19-CAR T cells results in B-cell depletion and signs of cytokine release syndrome. EMBO Mol. Med. *10*, e9158.

15. Jamali, A., Kapitza, L., Schaser, T., Johnston, I.C.D., Buchholz, C.J., and Hartmann, J. (2019). Highly Efficient and Selective CAR-Gene Transfer Using CD4- and CD8-Targeted Lentiviral Vectors. Mol. Ther. Methods Clin. Dev. *13*, 371–379.

16. Deng, Q., Han, G., Puebla-Osorio, N., Ma, M.C.J., Strati, P., Chasen, B., Dai, E., Dang, M., Jain, N., Yang, H., et al. (2020). Characteristics of anti-CD19 CAR T cell infusion products associated with efficacy and toxicity in patients with large B cell lymphomas. Nat. Med. *26*, 1878–1887.

17. Sheih, A., Voillet, V., Hanafi, L.A., DeBerg, H.A., Yajima, M., Hawkins, R., Gersuk, V., Riddell, S.R., Maloney, D.G., Wohlfahrt, M.E., et al. (2020). Clonal kinetics and single-cell transcriptional profiling of CAR-T cells in patients undergoing CD19 CAR-T immunotherapy. Nat. Commun. *11*, 219.

18. Bai, Z., Lundh, S., Kim, D., Woodhouse, S., Barrett, D.M., Myers, R.M., Grupp, S.A., Maus, M.V., June, C.H., Camara, P.G., et al. (2021). Single-cell multiomics dissection of basal and antigen-specific activation states of CD19-targeted CAR T cells. J. Immunother. Cancer *9*, e002328.

19. Boroughs, A.C., Larson, R.C., Marjanovic, N.D., Gosik, K., Castano, A.P., Porter, C.B.M., Lorrey, S.J., Ashenberg, O., Jerby, L., Hofree, M., et al. (2020). A Distinct Transcriptional Program in Human CAR T Cells Bearing the 4-1BB Signaling Domain Revealed by scRNA-Seq. Mol. Ther. *28*, 2577–2592.

20. Wang, X., Peticone, C., Kotsopoulou, E., Göttgens, B., and Calero-Nieto, F.J. (2021). Single-cell transcriptome analysis of CAR T-cell products reveals subpopulations, stimulation, and exhaustion signatures. OncoImmunology *10*, 1866287.

21. Arlt, A., and Schäfer, H. (2011). Role of the immediate early response 3 (IER3) gene in cellular stress response, inflammation and tumorigenesis. Eur. J. Cell Biol. *90*, 545–552.

22. Long, A.H., Haso, W.M., Shern, J.F., Wanhainen, K.M., Murgai, M., Ingaramo, M., Smith, J.P., Walker, A.J., Kohler, M.E., Venkateshwara, V.R., et al. (2015). 4-1BB costimulation ameliorates T cell exhaustion induced by tonic signaling of chimeric antigen receptors. Nat. Med. *21*, 581–590.

23. Al-Mutairi, M.S., Cadalbert, L.C., McGachy, H.A., Shweash, M., Schroeder, J., Kurnik, M., Sloss, C.M., Bryant, C.E., Alexander, J., and Plevin, R. (2010). MAP kinase phosphatase-2 plays a critical role in response to infection by Leishmania mexicana. PLoS Pathog. *6*, e1001192.

24. Haddock, A.N., Labuzan, S.A., Haynes, A.E., Hayes, C.S., Kakareka, K.M., and Waddell, D.S. (2019). Dual-specificity phosphatase 4 is upregulated during skeletal muscle atrophy and modulates extracellular signal-regulated kinase activity. Am. J. Physiol. Cell Physiol. *316*, C567–C581.

25. Uche, U.U., Piccirillo, A.R., Kataoka, S., Grebinoski, S.J., D'Cruz, L.M., and Kane, L.P. (2018). PIK3IP1/TrIP restricts activation of T cells through inhibition of PI3K/Akt. J. Exp. Med. *215*, 3165–3179.

26. van Spriel, A.B., Puls, K.L., Sofi, M., Pouniotis, D., Hochrein, H., Orinska, Z., Knobeloch, K.-P., Plebanski, M., and Wright, M.D. (2004). A regulatory role for CD37 in T cell proliferation. J. Immunol. *172*, 2953–2961.

27. Hwang, S.S., Lim, J., Yu, Z., Kong, P., Sefik, E., Xu, H., Harman, C.C.D., Kim, L.K., Lee, G.R., Li, H.-B., and Flavell, R.A. (2020). mRNA destabilization by BTG1 and BTG2 maintains T cell quiescence. Science *367*, 1255–1260.

28. Mair, F., Erickson, J.R., Voillet, V., Simoni, Y., Bi, T., Tyznik, A.J., Martin, J., Gottardo, R., Newell, E.W., and Prlic, M. (2020). A Targeted Multi-omic Analysis Approach Measures Protein Expression and Low-Abundance Transcripts on the Single-Cell Level. Cell Rep. *31*, 107499.

29. Erhard, F., Baptista, M.A.P., Krammer, T., Hennig, T., Lange, M., Arampatzi, P., Jürges, C.S., Theis, F.J., Saliba, A.-E., and Dölken, L. (2019). scSLAM-seq reveals core features of transcription dynamics in single cells. Nature *571*, 419–423.

30. Guéhenneux, F., Duret, L., Callanan, M.B., Bouhas, R., Hayette, S., Berthet, C., Samarut, C., Rimokh, R., Birot, A.M., Wang, Q., et al. (1997). Cloning of the mouse BTG3 gene and definition of a new gene family (the BTG family) involved in the negative control of the cell cycle. Leukemia *11*, 370–375.

31. Shi, J., Zhao, Y., Wang, Y., Gao, W., Ding, J., Li, P., Hu, L., and Shao, F. (2014). Inflammatory caspases are innate immune receptors for intracellular LPS. Nature *514*, 187–192.

32. Hornick, A.L., Li, N., Oakland, M., McCray, P.B., Jr., and Sinn, P.L. (2016). Human, Pig, and Mouse Interferon-Induced Transmembrane Proteins Partially Restrict Pseudotyped Lentiviral Vectors. Hum. Gene Ther. *27*, 354–362.

33. Zhao, X., Li, J., Winkler, C.A., An, P., and Guo, J.T. (2019). IFITM genes, variants, and their roles in the control and pathogenesis of viral infections. Front. Microbiol. *9*, 3228.

34. Li, K., Markosyan, R.M., Zheng, Y.M., Golfetto, O., Bungart, B., Li, M., Ding, S., He, Y., Liang, C., Lee, J.C., et al. (2013). IFITM proteins restrict viral membrane hemifusion. PLoS Pathog. *9*, e1003124.

35. Ozog, S., Timberlake, N.D., Hermann, K., Garijo, O., Haworth, K.G., Shi, G., Glinkerman, C.M., Schefter, L.E., D'Souza, S., Simpson, E., et al. (2019). Resveratrol trimer enhances gene delivery to hematopoietic stem cells by reducing antiviral restriction at endosomes. Blood *134*, 1298–1311.

36. Cocchi, F., DeVico, A.L., Garzino-Demo, A., Arya, S.K., Gallo, R.C., and Lusso, P. (1995). Identification of RANTES, MIP-1 α, and MIP-1 β as the major HIV-suppressive factors produced by CD8+ T cells. Science *270*, 1811–1815.

37. Nicolet, B.P., Guislain, A., van Alphen, F.P.J., Gomez-Eerland, R., Schumacher, T.N.M., van den Biggelaar, M., and Wolkers, M.C. (2020). CD29 identifies IFN-γ-producing human $CD8^+$ T cells with an increased cytotoxic potential. Proc. Natl. Acad. Sci. USA *117*, 6686–6696.

38. Klebanoff, C.A., Gattinoni, L., Torabi-Parizi, P., Kerstann, K., Cardones, A.R., Finkelstein, S.E., Palmer, D.C., Antony, P.A., Hwang, S.T., Rosenberg, S.A., et al. (2005). Central memory self/tumor-reactive CD8+ T cells confer superior antitumor immunity compared with effector memory T cells. Proc. Natl. Acad. Sci. USA *102*, 9571–9576.

39. Li, F., and Zhang, H. (2019). Lysosomal Acid Lipase in Lipid Metabolism and Beyond. Arterioscler. Thromb. Vasc. Biol. *39*, 850–856.

40. Hah, Y.S., Noh, H.S., Ha, J.H., Ahn, J.S., Hahm, J.R., Cho, H.Y., and Kim, D.R. (2012). Cathepsin D inhibits oxidative stress-induced cell death via activation of autophagy in cancer cells. Cancer Lett. *323*, 208–214.

41. Weidner, T., Agarwal, S., Perian, S., Fusil, F., Braun, G., Hartmann, J., Verhoeyen, E., and Buchholz, C.J. (2021). Genetic in vivo engineering of human T lymphocytes in mouse models. Nat. Protoc. *16*, 3210–3240.

42. Agarwal, S., Hanauer, J.D.S., Frank, A.M., Riechert, V., Thalheimer, F.B., and Buchholz, C.J. (2020). In Vivo Generation of CAR T Cells Selectively in Human $CD4^+$ Lymphocytes. Mol. Ther. *28*, 1783–1794.

43. Liu, H., Han, H., Li, J., and Wong, L. (2003). An in-silico method for prediction of polyadenylation signals in human sequences. Genome informatics. International Conference on Genome Informatics *14*, 84–93.

44. Stuart, T., Butler, A., Hoffman, P., Hafemeister, C., Papalexi, E., Mauck, W.M., 3rd, Hao, Y., Stoeckius, M., Smibert, P., and Satija, R. (2019). Comprehensive Integration of Single-Cell Data. Cell *177*, 1888–1902.e21.

45. Wickham, H. (2016). ggplot2: Elegant Graphics for Data Analysis (Springer-Verlag).

46. Clarke, D.J.B., Jeon, M., Stein, D.J., Moiseyev, N., Kropiwnicki, E., Dai, C., Xie, Z., Wojciechowicz, M.L., Litz, S., Hom, J., et al. (2021). Appyters: Turning Jupyter Notebooks into data-driven web apps. Patterns (NY) *2*, 100213.

47. Ameijeiras-Alonso, J., Crujeiras, R.M., and Rodriguez-Casal, A. (2021). multimode: An R Package for Mode Assessment. J. Stat. Softw. *97*, 1–32.

48. Barrett, T., Wilhite, S.E., Ledoux, P., Evangelista, C., Kim, I.F., Tomashevsky, M., Marshall, K.A., Phillippy, K.H., Sherman, P.M., Holko, M., et al. (2013). NCBI GEO: archive for functional genomics data sets–update. Nucleic Acids Res. *41*, D991–D995.

OMTM, Volume *23*

Supplemental information

Monitoring CAR T cell generation with a CD8-targeted lentiviral vector by single-cell transcriptomics

Filippos T. Charitidis, Elham Adabi, Frederic B. Thalheimer, Colin Clarke, and Christian J. Buchholz

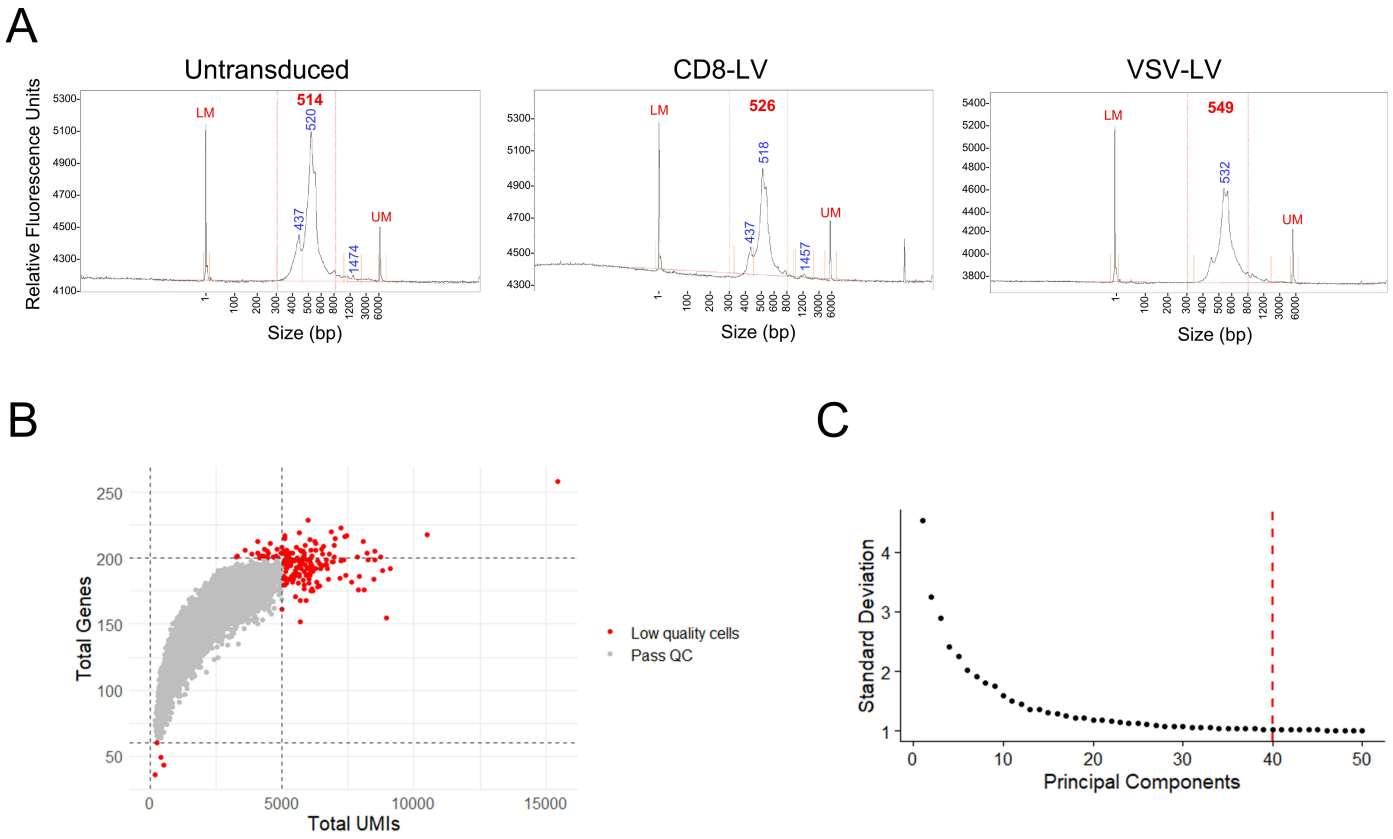

Figure S1: Quality control and pre-processing.
(**A**) Quality control of final sequencing libraries by Fragment Analyzer. The average sizes of the libraries were measured within the indicated area of 300-800 base-pairs (bp) and are shown in red numbers. Lower marker (LM) and upper marker (UM) fragments are indicated. (**B**) Overlay of cells from all groups are shown. Low quality cells (red) were filtered out. (**C**) Elbowplot selecting the top 40 principal components for UMAP analysis.

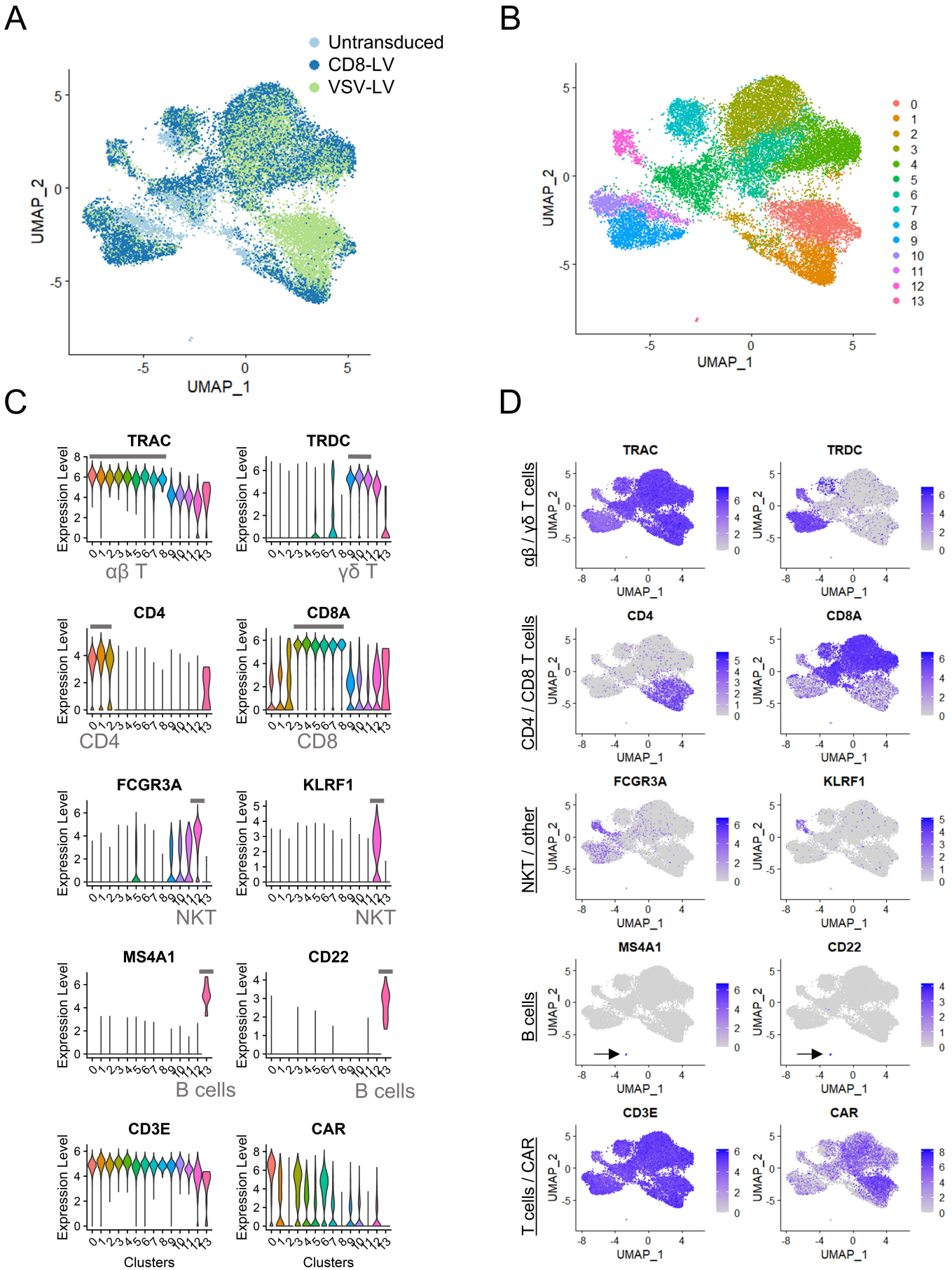

Figure S2: Clustering and identification of major immune subtypes in UMAP plots. (**A**) Overlapping merged samples in the UMAP plot. (**B**) Unsupervised clustering analysis and projection of clusters on UMAP plot, identified by the functions of *FindNeightbors* and *FindClusters.* (**C**) Expression of major T cell marker genes across the clusters. (**D**) UMAP plots of all samples merged, visualizing the localization of major immune cell types. Arrows indicate the location of B cells into the plots.

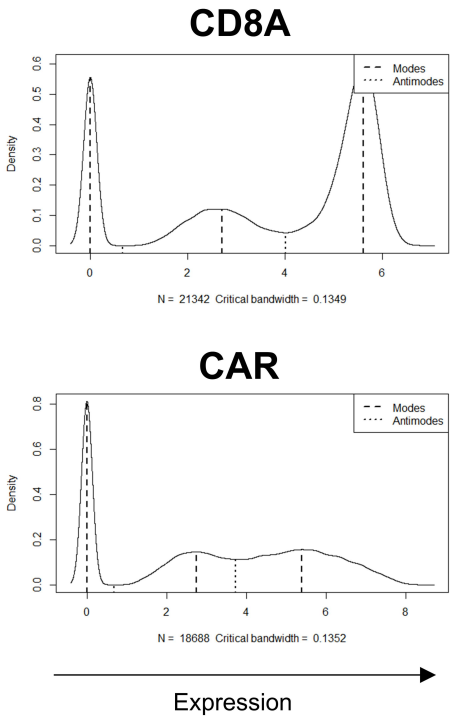

Figure S3: Multimodal analysis.
Multimodal analysis on density of data points across the normalized expression of *CD8A* or *CAR* genes, on total samples or transduced samples, respectively, calculated by the package *multimode*. Modes are shown in dashed lines, while antimodes in dotted lines.

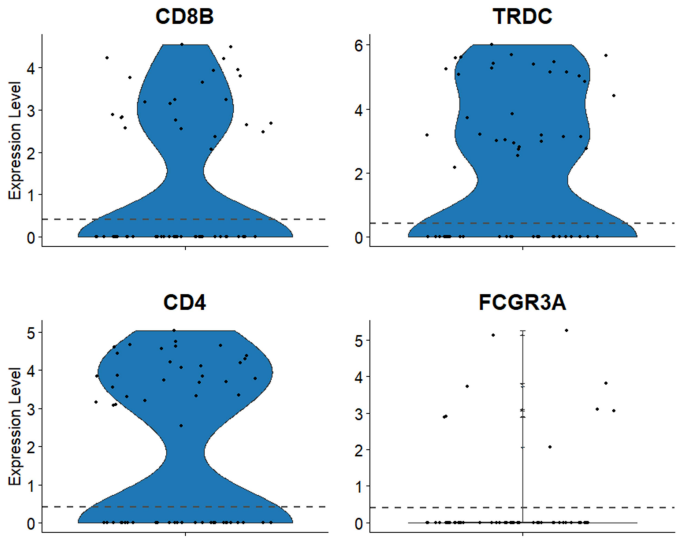

Figure S4: Violin plots of marker gene expression of potential off-target cells in CD8-LV sample.
Identification of cell types present in *CAR^{high} CD8A$^{neg/low}$* cells generated with CD8-LV, based on the expression of *CD8B*, *TRDC*, *CD4* and *FCGR3A* (referring to 1.26% of cells shown in Fig. 2D). Dashed lines indicate the lower cutoff for determining the cells positive for the plotted marker. Cell number for each cell type is shown in Table 2.

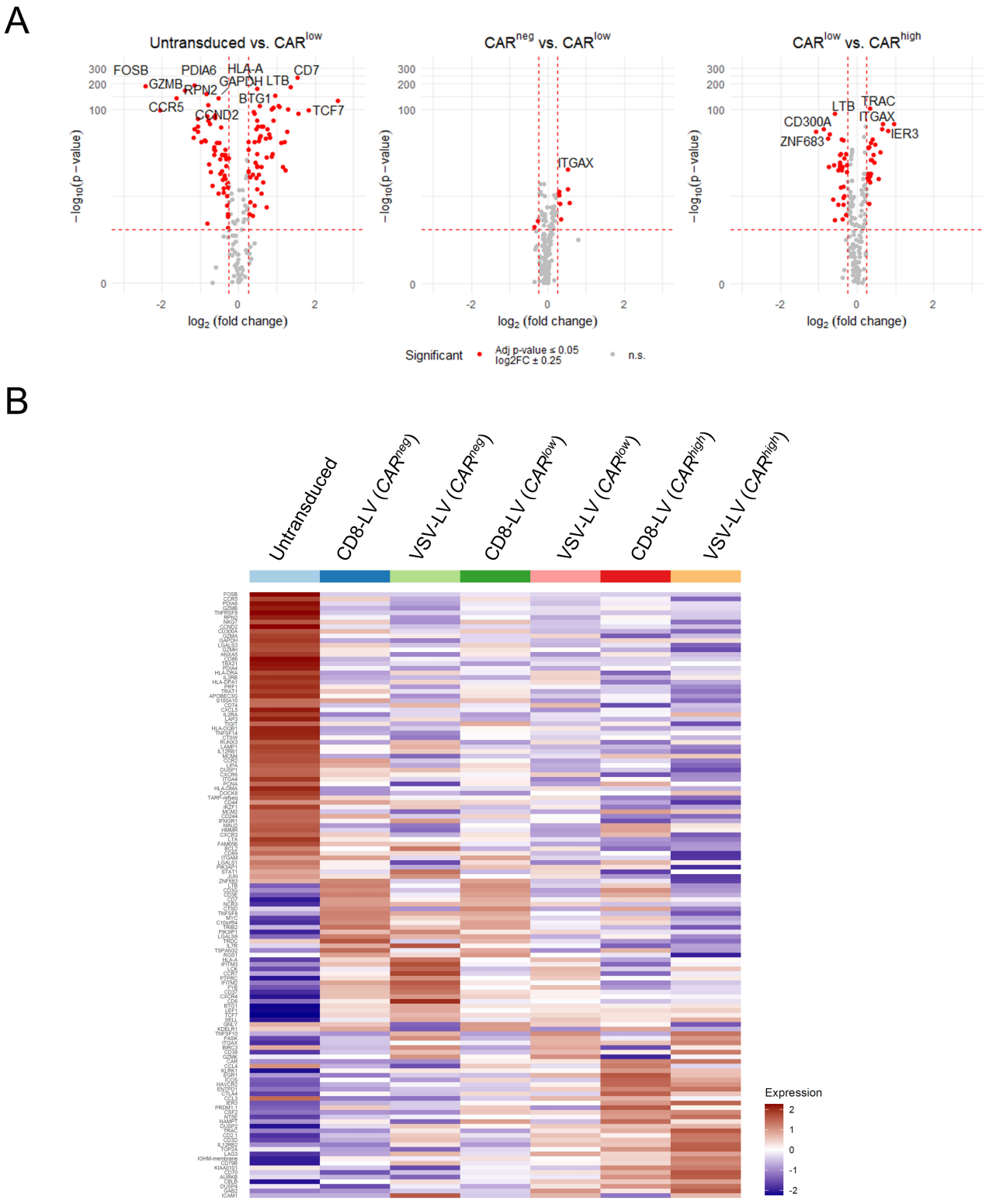

Figure S5. Comparisons of *CAR^{neg}*, *CAR^{low}* and *CAR^{high}* cells.
(**A**) Volcano plots of CD8+ CAR^{neg} versus CAR^{low} cells (left) and CD8+ *CAR^{low}* versus *CAR^{high}* cells (right). (**B**) Heatmap plot of upregulated genes between untransduced, *CAR^{neg}*, *CAR^{low}* and *CAR^{high}* identified by *FindAllMarkers* function in Seurat (log2FC ± 0.25, adj.p-value <0.05).

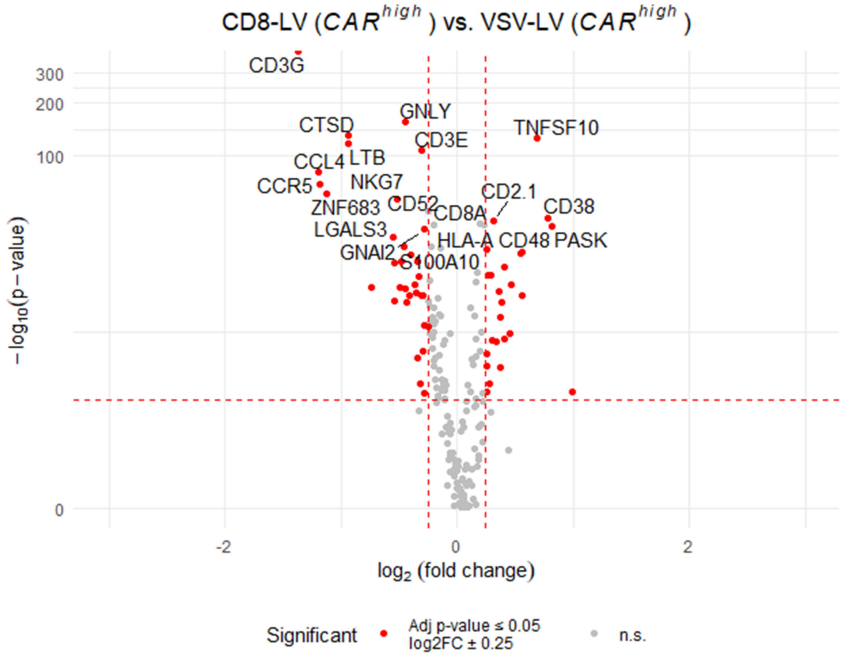

Figure S6. Volcano plot of comparing *CAR^{high}* cells generated by the two vectors.
Volcano plots of CD8+ *CAR^{high}* cells generated by either CD8-LV or VSV-LV showing the differentially expressed genes identified by *FindMarkers* function in Seurat.

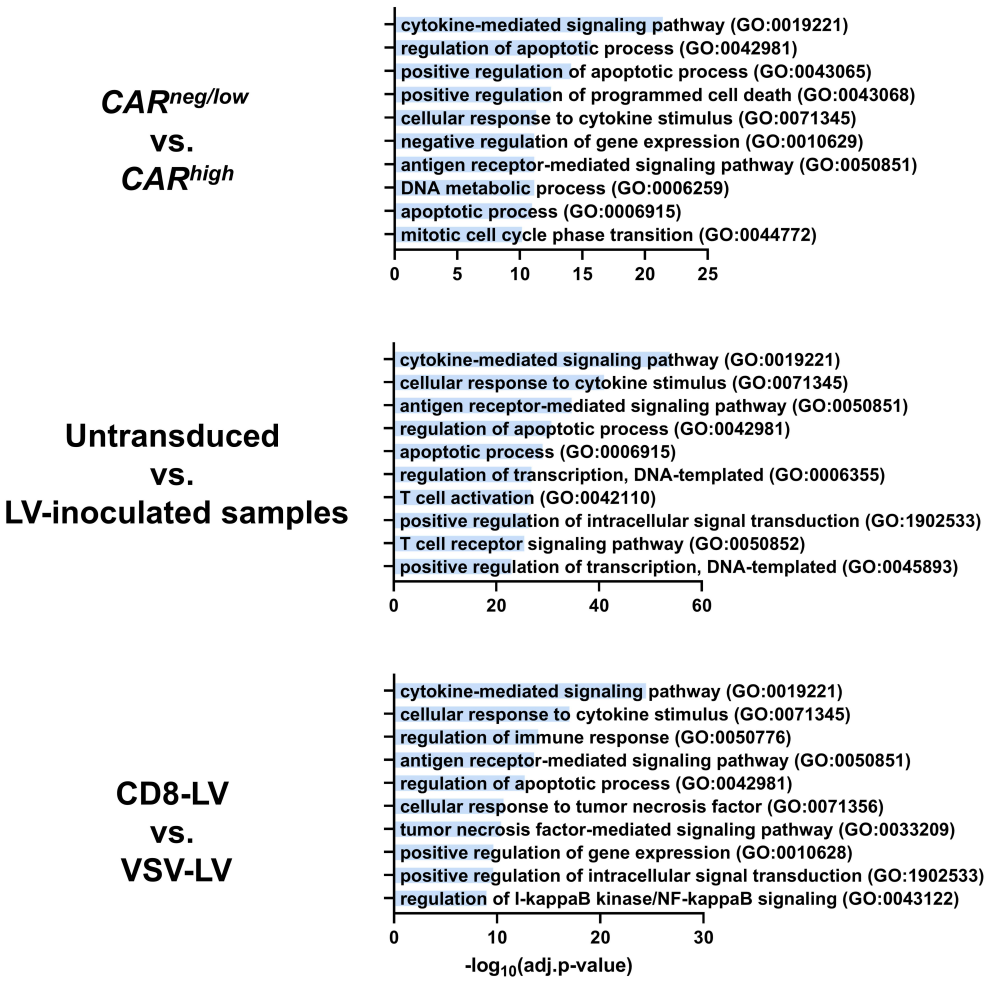

Figure S7. Gene set enrichment analysis.
Gene set enrichment analysis of differentially expressed genes identified in the indicated comparisons with the gene sets of Gene Ontology (GO) Biological Process database. Top 10 results in each category are plotted. LV-inoculated samples: concatenated CD8-LV and VSV-LV samples.

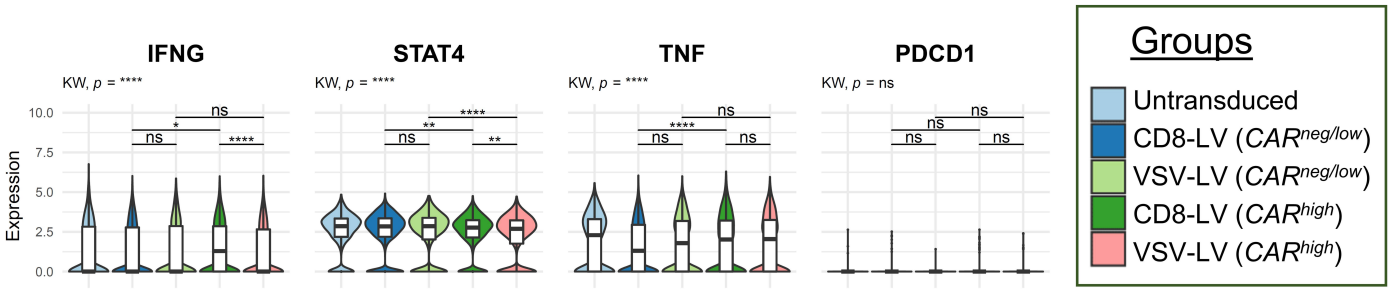

Figure S8. Supplemental violin plots.
Unaltered expression of particular genes of interest (KW: Kruskal-Wallis multiple comparison test. Wilcoxon Rank Sum test performed for paired-wise comparisons, p-values adjusted based on Bonferroni. ns: non-significant, * < 0.05, ** < 0.01, *** < 0.001, **** < 0.0001).

S1 Table. Metrics of cells pre- and post-filtering in scRNA-seq analysis.

	Untransduced	CD8-LV	VSV-LV
Unfiltered cells	2711	9793	9023
Post-filtered cells	2654	9713	8975
Total removed cells	57	80	48
Proportion of removed cells	2.10 %	0.82 %	0.53 %